

# Theoretical study of projectile fragmentation in $^{112}\text{Sn} + ^{112}\text{Sn}$ and $^{124}\text{Sn} + ^{124}\text{Sn}$ reactions at 1 GeV/nucleon

H. Imal, A. Ergun, N. Buyukcizmeci, and R. Ogul

*Department of Physics, University of Selçuk, 42079 Konya, Turkey*

A.S. Botvina

*Frankfurt Institute for Advanced Studies, J.W. Goethe University, D-60438 Frankfurt am Main, Germany and*

*Institute for Nuclear Research, Russian Academy of Sciences, 117312 Moscow, Russia*

W. Trautmann

*GSI Helmholtzzentrum für Schwerionenforschung GmbH, D-64291 Darmstadt, Germany*

(Dated: September 16, 2021)

We analyze the production cross sections and isotopic distributions of projectile-like residues in the reactions  $^{112}\text{Sn} + ^{112}\text{Sn}$  and  $^{124}\text{Sn} + ^{124}\text{Sn}$  at an incident beam energy of 1 GeV/nucleon measured with the FRS fragment separator at the GSI laboratory. Calculations within the statistical multifragmentation model (SMM) for an ensemble of excited sources were performed with ensemble parameters determined previously for similar reactions at 600 MeV/nucleon. The obtained good agreement with the experiment establishes the universal properties of the excited spectator systems produced during the dynamical stage of the reaction. It is furthermore confirmed that a significant reduction of the symmetry-energy term at the freeze-out stage of reduced density and high temperature is necessary to reproduce the experimental isotope distributions. A trend of decreasing symmetry energy for large neutron-rich fragments of low excitation energy is interpreted as a nuclear-structure effect.

PACS numbers: 25.70.-z, 25.70.Pq

## I. INTRODUCTION

The study of nuclear fragmentation and multifragmentation reactions is of particular interest due to both, their important practical applications as well as the new research opportunities that these reactions provide. The latter include the investigation of the equation of state of nuclear matter, of the composition of nuclear matter at subnuclear densities, and of phase transitions in nuclear systems. Information of this kind can be related to processes taking place during the collapse and explosion of massive stars and in the formation of neutron stars [1, 2]. The isospin composition of the produced fragments has been found to be especially important because it can be used for determining the strength of the symmetry energy during fragment formation in the hot and diluted environment [3–6], which is crucial for weak reaction rates in stellar matter [2].

Mid-peripheral heavy-ion collisions at relativistic energies provide us with the possibility to study the production of isotopes as a result of fragmentation and multifragmentation of the colliding nuclei. Recently, experiments for two symmetric systems  $^{124}\text{Sn} + ^{124}\text{Sn}$  and  $^{112}\text{Sn} + ^{112}\text{Sn}$ , both at an incident energy of 1 GeV/nucleon, were performed by the FRS collaboration at the GSI laboratory [7]. The high-resolution magnetic FRagment Separator (FRS) was used for the separation and identification of the reaction products. The initial neutron to proton ratios ( $N/Z$ ) of the symmetric systems are 1.24 for  $^{112}\text{Sn}$  and 1.48 for  $^{124}\text{Sn}$ . The measured isotopic cross sections of identified fragments from these two

reactions are reported in tabulated form in Ref. [7].

In a previous study with the ALADIN forward-spectrometer, the fragmentation of stable  $^{124}\text{Sn}$  and radioactive  $^{107}\text{Sn}$  and  $^{124}\text{La}$  projectiles at 600 MeV/nucleon has been measured and analyzed [6]. In particular, it was found that the charge and isotope yields, fragment multiplicities and temperatures, and correlations of various fragment properties can be well described within the Statistical Multifragmentation Model (SMM, Ref. [8]). An ensemble of excited sources was assumed to represent the collision systems after the initial non-equilibrium part of the reaction and chosen as starting configuration for the statistical description of the subsequent reaction stages. Its general form in the plane of source mass and excitation energy was adapted from previous studies [9–11] and the sensitivity of the experimental observables to the parameters required for the liquid-drop description of the primary excited fragments was evaluated [6]. With the present work, we demonstrate that the same approach can be used to describe the recent FRS data for similar projectiles and that comparable results concerning the required model parameters are obtained. With the new FRS data, the analysis can be extended to include the distributions of heavier isotopes up to close to the initial projectile mass.

As shown previously, the symmetry energy represents the main model parameter governing the mean  $N/Z$  values, the isoscaling parameters, and the isotopic composition of the fragment yields. For more violent collisions associated with larger particle and fragment multiplicities, its strength needs to be reduced if an ad-

equate description of the experimental data is to be achieved [5, 6, 12, 13]. This observation was also made in the analysis of the experimental data of Liu et al. [14] obtained at the MSU laboratory for the same projectiles and targets that were studied with the FRS, i.e.  $^{124}\text{Sn} + ^{124}\text{Sn}$  and  $^{112}\text{Sn} + ^{112}\text{Sn}$ , but at the lower energy of 50 MeV/nucleon [15–17].

## II. STATISTICAL APPROACH TO MULTIFRAGMENTATION

It has been repeatedly demonstrated that the statistical multifragmentation model (SMM, Ref. [8]) is a useful tool for describing the fragment production in peripheral heavy-ion collisions at high energy [6, 10, 11, 18]. In the present work, we consider the ensemble approach with the same parameters that were used for the interpretation of the ALADIN data [6]. The general properties of the considered ensembles of residual nuclei, found to be quite adequate for describing the multifragmentation of relativistic projectiles, are given in Ref. [10]. The excited residues form a broad distribution in the energy vs. mass plane, extending from large masses near the projectile mass and low excitation energies up to sources of small mass but high excitation energy in the vicinity of the nucleon binding energies. The  $N/Z$  ratios of the sources are taken to be those of the initial projectiles.

In the SMM, it is assumed that a statistical equilibrium is reached within a low-density freeze-out zone. The breakup channels are composed of nucleons and nuclear fragments, and the conservation laws (energy, momentum, angular momentum, mass number  $A$  and atomic number  $Z$ ) are taken into consideration. Besides the breakup channels, the compound-nucleus channels are also included, and the competition between all channels is permitted. In this way, the SMM covers the conventional evaporation and fission processes occurring at low excitation energy as well as the transition region between the low and high energy de-excitation regimes. In the thermodynamic limit, the SMM is consistent with a liquid-gas type phase transition in which the liquid phase is represented by an infinite nuclear cluster [19], permitting the connection with the astrophysical case [20].

For finite nuclear systems, the SMM version developed in Refs. [8, 21, 22] is used. It represents the main version used previously for successful comparisons with a variety of experimental data [6, 10, 11, 18, 23–25]. We calculate the contributions of all breakup channels partitioning the system into various species. The decay channels are generated by a Monte Carlo method according to their statistical weights. Light fragments with mass number  $A \leq 4$  and charge number  $Z \leq 2$  are considered as elementary particles (nuclear gas) with their corresponding spins and translational degrees of freedom. The fragments with mass number  $A > 4$  are treated as heated nuclear liquid-drops. In this way one can study the nuclear liquid-gas coexistence in the freeze-out volume. The

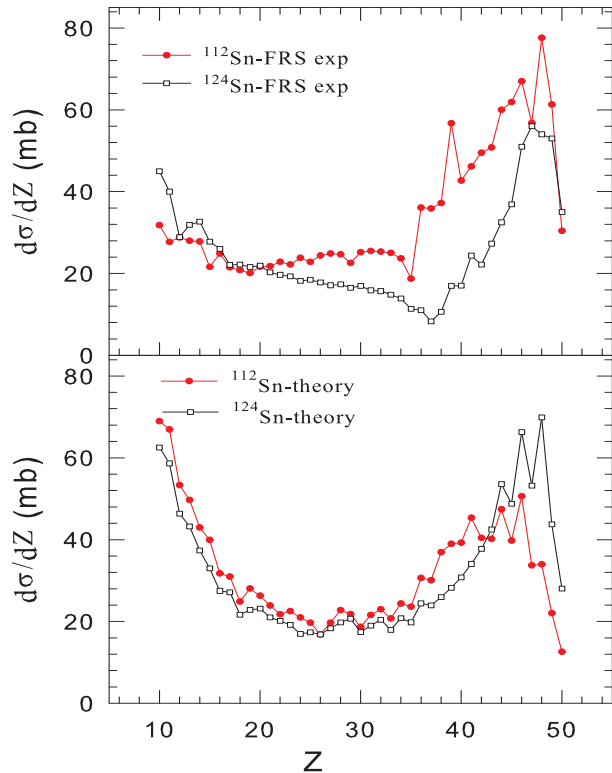


FIG. 1: (color online) Top panel: production cross sections of the measured projectile fragments as a function of the fragment atomic number  $Z$  for the two reactions (from Ref. [7]). Bottom panel: the corresponding distributions as obtained from ensemble calculations with standard parameters (for details see text in Section II).

free energies  $F_{A,Z}$  of fragments are parameterized as the sums of the bulk, surface, Coulomb and symmetry energy contributions

$$F_{A,Z} = F_{A,Z}^B + F_{A,Z}^S + E_{A,Z}^C + E_{A,Z}^{sym}. \quad (1)$$

The bulk contribution is given by  $F_{A,Z}^B = (-W_0 - T^2/\varepsilon_0)A$ , where  $T$  is the temperature, the parameter  $\varepsilon_0$  is related to the level density, and  $W_0 = 16$  MeV is the binding energy of infinite nuclear matter. The contribution of the surface energy is  $F_{A,Z}^S = B_0 A^{2/3} [(T_c^2 - T^2)/(T_c^2 + T^2)]^{5/4}$ , where  $B_0 = 18$  MeV is the surface energy term, and  $T_c = 18$  MeV the critical temperature of infinite nuclear matter. The Coulomb contribution is  $E_{A,Z}^C = c Z^2 / A^{1/3}$ , where  $c$  denotes the Coulomb parameter obtained in the Wigner-Seitz approximation,  $c = (3/5)(e^2/r_0)(1 - (\rho/\rho_0)^{1/3})$ , with the charge unit  $e$ ,  $r_0 = 1.17$  fm, and the normal nuclear-matter density  $\rho_0 = 0.15$  fm $^{-3}$ . And finally, the symmetry term is  $E_{A,Z}^{sym} = \gamma(A - 2Z)^2 / A$ , where  $\gamma = 25$  MeV is the symmetry energy parameter. All the parameters given above are taken from the Bethe-Weizsäcker formula and

correspond to the assumption of isolated fragments with normal density unless their modifications in the hot and dense freeze-out configuration follow from the analysis of experimental data. For the freeze-out density, one-third of the normal nuclear matter density is assumed, as in previous studies and qualitatively consistent with independent experimental determinations [26, 27].

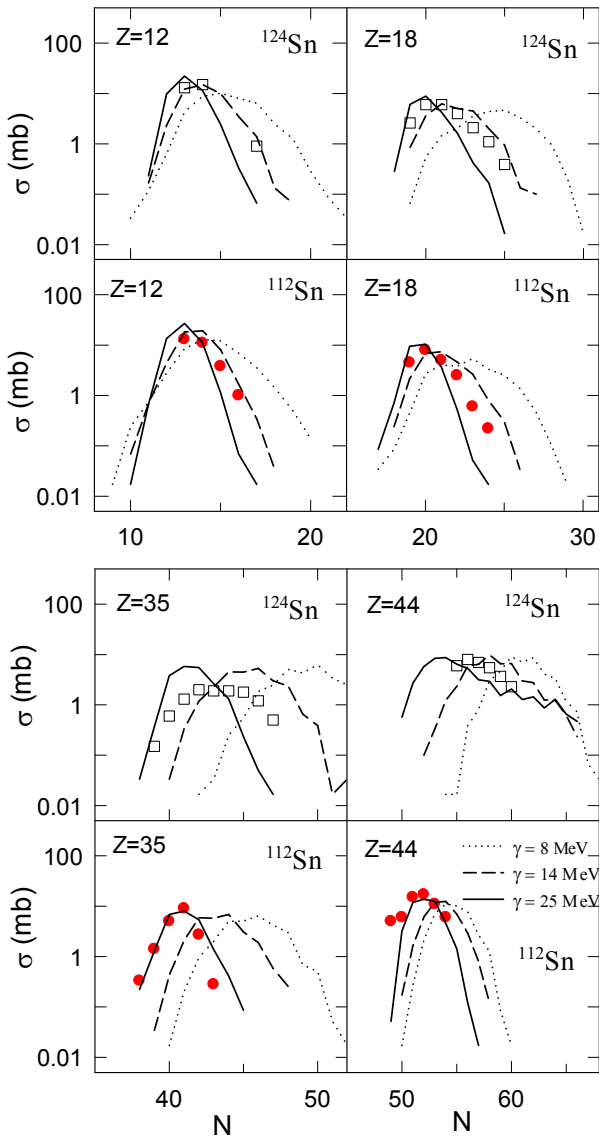


FIG. 2: (color online) Predicted (lines) and measured (symbols, from Ref. [7]) isotope distributions for final fragments of the projectiles  $^{124}\text{Sn}$  and  $^{112}\text{Sn}$  with atomic numbers  $Z = 12, 18, 35$ , and  $44$ . Calculations are shown for three different choices of the symmetry-term coefficient  $\gamma = 8$  (dotted),  $14$  (dashed), and  $25$  MeV (full lines).

After formation in the freeze-out volume the hot fragments undergo secondary de-excitation and propagate in the mutual Coulomb field. Their secondary decay

includes evaporation, fission, and Fermi-break-up processes. The corresponding models are similar to those used for the description of low energy reactions [8, 22, 28]; they do account, however, for modifications of fragment properties under freeze-out conditions [29, 30].

Especially, the modification of the fragment symmetry energy must be taken into account in the first de-excitation steps, as the hot fragments are still surrounded by other species. At the end of the evaporation cascade, the standard properties will have to be restored as explicitly described in Ref. [30]. In the calculations, this is realized with a linear interpolation between these two limiting cases in the interval of excitation energies below  $E_x^{\text{int}} = 1$  MeV/nucleon. In this interval, the mass of a nucleus with mass and atomic numbers  $A$  and  $Z$  evolves with the excitation energy  $E_x$  as

$$m_{A,Z} = m_{ld}(\gamma) \cdot x + m_{st} \cdot (1 - x) \quad (2)$$

where  $x = E_x/A/E_x^{\text{int}}$  and  $x \leq 1$ . The excitation energy  $E_x$  is determined from the energy balance, taking into account the mass  $m_{A,Z}$  at the given excitation. The liquid-drop mass  $m_{ld}$  is that of hot fragments as adopted in the SMM (without temperature and density dependences),

$$m_{ld}(\gamma) = m_n(A - Z) + m_p Z - AW_0 + B_0 A^{2/3} + \gamma \frac{(A - 2Z)^2}{A} + \frac{3e^2 Z^2}{5r_0 A^{1/3}}, \quad (3)$$

where  $m_n$  and  $m_p$  are the masses of free neutrons and protons and  $W_0$  and  $B_0$  the volume and surface term coefficients, respectively.

The standard masses  $m_{st}$  are taken from the nuclear mass tables or, if experimental masses are not available, the mass formula of Myers and Swiatecki [31] is used. It has also been confirmed that, with the standard symmetry-term coefficient  $\gamma = 25$  MeV, the interpolation procedure leads to very similar results as a standard evaporation that uses the ground-state masses  $m_{st}$  throughout.

### III. CHARGE AND ISOTOPIC DISTRIBUTIONS

Cross sections for projectile fragmentation in the two studied reactions  $^{124}\text{Sn} + ^{124}\text{Sn}$  and  $^{112}\text{Sn} + ^{112}\text{Sn}$  at 1 GeV/nucleon are shown in Fig. 1 as a function of the atomic number  $Z$  of the final fragments. The experimental results (top panel) are obtained by summing up the isotope yields given in the tables of Ref. [7]. The bottom panel shows the theoretical results obtained from ensemble calculations performed for 500 000 reaction events with the standard SMM parameters given in Section II and with the ensemble parameters used in the analysis of the ALADIN data in Ref. [6]. To permit a more quantitative comparison of the model results with the experimental data, the SMM ensemble calculations were globally normalized with respect to the measured elemental

cross sections in the interval  $20 \leq Z \leq 25$ . The obtained factors are 0.00334 mb and 0.00344 mb per theoretical event for  $^{124}\text{Sn}$  and  $^{112}\text{Sn}$  projectiles, respectively. The observed agreement between the experimental and theoretical results is, at most, qualitative and considerable differences exist. For  $^{124}\text{Sn}$  in particular, the measured yields in the range  $30 \leq Z \leq 45$  seem low, with respect to the calculations as well as relative to the experimental yields for  $^{112}\text{Sn}$ . To a large extent, this is due to the fact that the isotope distributions were not always fully covered in the experiment, thus causing the observed distortions of the  $Z$  distributions from their known general form in high-energy reactions (see, e.g., Refs. [8, 32, 33]).

Cross section differences are also observed for individual isotopes from different experiments. For example, Föhr et al. [7] report a cross section of  $19 \pm 4$  mb for the production of  $^{22}\text{Ne}$  in the fragmentation of  $^{124}\text{Sn}$  projectiles at 1 GeV/nucleon while the corresponding cross section reported by Ogul et al. [6] for the same reaction at 600 MeV/nucleon is approximately 40 mb. A decrease with energy is not expected but it has to be considered that the solid-angle acceptance of the FRS is much smaller than that of the ALADIN spectrometer and that, when evaluating the total production cross sections for intermediate mass fragments (IMF), the assumption of an isotropic emission in the rest frame of the considered species was adopted in Ref. [7]. This leads to an underestimation if the transverse momentum distributions are wider than the longitudinal distributions that are actually measured with the FRS. Anisotropies of this kind may be caused by a side-motion of the excited projectile residues after the dynamical reaction stage that is especially seen in the multifragmentation regime [34, 35]. The velocity characteristics of fragments previously investigated with the FRS show the effects of entering into the multifragmentation regime [36], and the problem of underestimating the yields of fragments with  $Z \lesssim 14$  is admitted in Ref. [7]. For these reasons, less weight is given to the absolute IMF yields in the present analysis which, in the following, will be focussed on the relative isotope distributions.

The parameter dependence of the predicted fragment yields was investigated in detail previously [6]. Both, the parameterization of the ensemble of hot sources as well as the description of the produced fragments in the hot environment were included in this study. It was found that possible modifications of the symmetry-energy term appear rather exclusively in the width and positions of the fragment isotopic distributions while other observables as, e.g., fragment multiplicities or  $Z$  distributions, are not particularly affected. For the present case, this is illustrated in Fig. 2 which shows the variation of the calculated isotopic distributions with the symmetry-energy coefficient  $\gamma$  for the final fragments with  $Z = 12, 18, 35$  and 44. The neutron numbers of the strongest isotope of an element and the widths of the distributions vary strongly with the  $\gamma$  parameter. A reduced  $\gamma$  causes the isotope distributions to be wider. It also leads to a

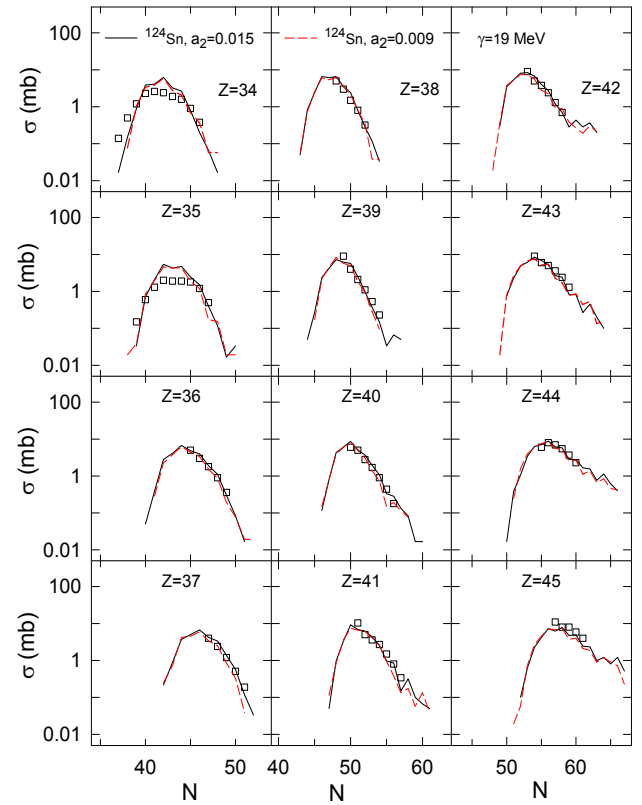


FIG. 3: (color online) Predicted isotopic cross-sections for final fragments with atomic numbers  $34 \leq Z \leq 45$  from the fragmentation of  $^{124}\text{Sn}$  projectiles for two ensemble parameters  $a_2 = 0.015 \text{ MeV}^{-2}$  (full line) and  $a_2 = 0.009 \text{ MeV}^{-2}$  (dashed) in comparison with the experimental data from Ref. [7] (open squares). The symmetry-term coefficient  $\gamma = 19 \text{ MeV}$  was used.

larger neutron content of the final fragments since the probability for charged-particle emission during the secondary de-excitation of neutron-rich primary fragments becomes higher [6, 29, 30]. The measured yields are best reproduced with  $\gamma = 14 \text{ MeV}$  in the case of the lightest fragments with  $Z = 12$  while the standard  $\gamma = 25 \text{ MeV}$  seems more appropriate for  $Z = 44$ .

Comparing the  $^{124}\text{Sn}$  and  $^{112}\text{Sn}$  fragmentations, the measured distributions are very similar for the lighter fragments ( $Z = 12, 18$ ), shifted with respect to each other by approximately one mass unit, but qualitatively different for the heavier species which are not produced in multifragmentation. The mass distributions of the  $Z = 35$  and 44 fragments are relatively narrow in good agreement with the predictions for  $\gamma = 25 \text{ MeV}$  in the case of the  $^{112}\text{Sn}$  fragmentation but much wider with a tail to larger mass numbers for  $^{124}\text{Sn}$ . This had already been noticed by the authors of Ref. [7] and was explained by showing the overall good agreement of the yield distributions with the predictions obtained from the empirical EPAX parametrization [37]. As shown by Charity [38],

the EPAX yield distributions approach the evaporation-attractor-line (EAL) if the excitation energies of the primary residues are sufficiently high, so that neutron and charged-particle evaporation will effectively compete. In the present case, the EAL is more easily reached from the neutron-poor  $^{112}\text{Sn}$  residues and, in fact, the most probable isotopes are found to lie close to this line as obtained with GEMINI evaporation calculations by Charity [38] or, equivalently, also with the secondary-evaporation calculations implemented in the SMM. The lighter fragments from  $^{124}\text{Sn}$  ( $Z = 12$  and  $18$ ) are also very close but a memory effect is clearly observed, reminiscent of the neutron richness of the initial sources.

For neutron-rich nuclei with lower excitations, neutron evaporation dominates and the mass number of the final product nucleus will be mainly determined by its initial excitation energy. While this is valid for individual source nuclei it does not affect much the final isotope distributions resulting from the ensemble of excited sources studied here. This has been confirmed with test calculations using varying ensemble parameters which show that the variations of the de-excitation chains are compensated by the change of the distribution of source nuclei populating a particular element. An example is given in Fig. 3 which presents the results for products with  $34 \leq Z \leq 45$  from  $^{124}\text{Sn}$  fragmentation for ensembles generated with parameters  $a_2 = 0.015$  (the standard value) and  $0.009 \text{ MeV}^{-2}$ . This parameter determines the curvature in the expression

$$A_s/A_0 = 1 - a_1(E_x/A_s) - a_2(E_x/A_s)^2 \quad (4)$$

describing the average mass number  $A_s$  of the equilibrated sources as a function of their excitation energy  $E_x$  (in MeV). Here  $A_0$  is the projectile mass and the parameter  $a_1$  is taken as  $a_1 = 0.001 \text{ MeV}^{-1}$ . The smaller value for  $a_2$  produces an ensemble with higher excitation energy, amounting to an increase  $\Delta E_x/A = 0.4$  to  $0.8 \text{ MeV}$  for source nuclei with mass numbers larger than about 90% of the projectile mass (cf. Fig. 5 in Ref. [6]). The resulting modifications of the isotope distributions are, apparently, very small. As a consequence, also the isotope distributions for heavier fragments from the  $^{124}\text{Sn}$  fragmentation, peaking several mass units away from the EAL ( $Z = 35$  and  $44$  shown in Fig. 2), retain their sensitivity to the strength of the symmetry energy.

The evolution of the final isotope distributions with atomic numbers from  $Z = 10$  to  $Z = 45$  is shown in Figs. 4 - 6 in a direct comparison of the neutron-rich and neutron-poor cases. The corresponding predictions had been calculated with standard parameters as, e.g.,  $a_2 = 0.015 \text{ MeV}^{-2}$  and  $B_0 = 18 \text{ MeV}$  and with various symmetry-energy coefficients  $\gamma$ . In the figures, they are shown for the  $\gamma$  values found to be most adequate for the selected five groups of elements listed in Table I. As expected from Fig. 2, the favored symmetry-term coefficient increases from  $\gamma = 16 \text{ MeV}$  for  $Z = 10 - 17$  to  $\gamma = 25 \text{ MeV}$  for  $Z = 38 - 45$  and  $^{112}\text{Sn}$ . In the case of  $^{124}\text{Sn}$ , the obtained  $\gamma$  values are similar for the smaller

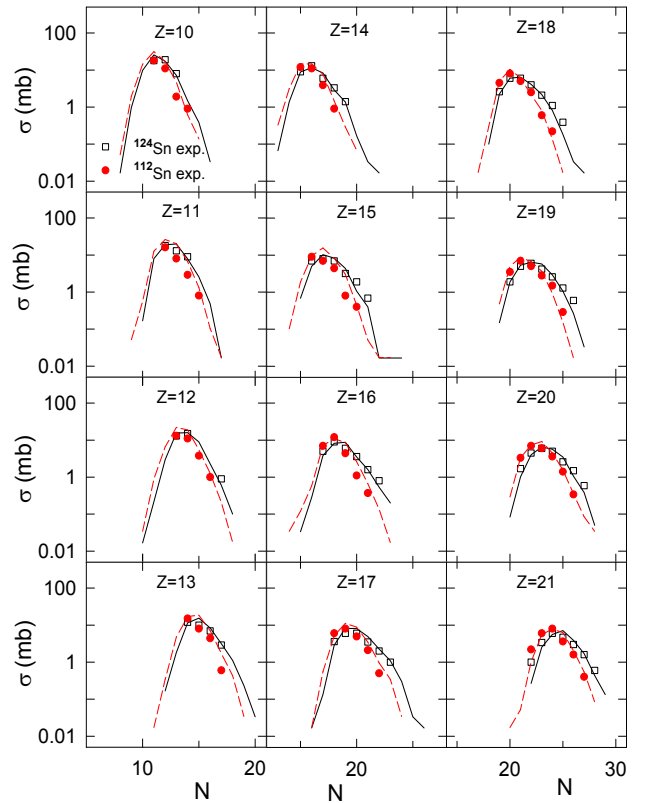


FIG. 4: (color online) Predicted (lines) and measured (symbols, from Ref. [7]) isotopic cross-sections for final fragments with atomic numbers  $10 \leq Z \leq 21$  from the fragmentation of  $^{124}\text{Sn}$  (open squares and full lines) and  $^{112}\text{Sn}$  projectiles (closed circles and dashed lines). The symmetry-term coefficients  $\gamma$  used in the calculations are given in Table I.

fragments but don't exceed  $\gamma = 20 \text{ MeV}$  as the fragment  $Z$  approaches that of the projectile.

The agreement of the calculated cross sections with the measured data is, overall, very satisfactory. We emphasize again that the calculations are obtained with the parameter set determined in the analysis of the ALADIN fragmentation data [6] and with a global normalization in the cross section interval  $20 \leq Z \leq 25$ . In particular also the yields of heavier isotopes with atomic numbers  $Z \approx 35$  to  $45$  are quite well reproduced (Fig. 6). Here, in the case of  $^{124}\text{Sn}$ , the isotopic distributions were only partly covered in the experiment which explains why the integrated cross sections appear rather low in this part of the  $Z$  spectrum (Fig. 1). It has also the effect that the determination of the optimum  $\gamma$  value is more difficult in the neutron-rich case. Except for  $Z = 35$  and  $44$ , the maxima of the isotopic yield distributions are not unambiguously determined (Fig. 6). It is only because of the larger sensitivity (cf. Fig. 2) that the precision is still of the order of  $\Delta\gamma = \pm 1$  also for  $^{124}\text{Sn}$ .

The FRS data are inclusive but smaller fragments are, nevertheless, known to be predominantly produced in

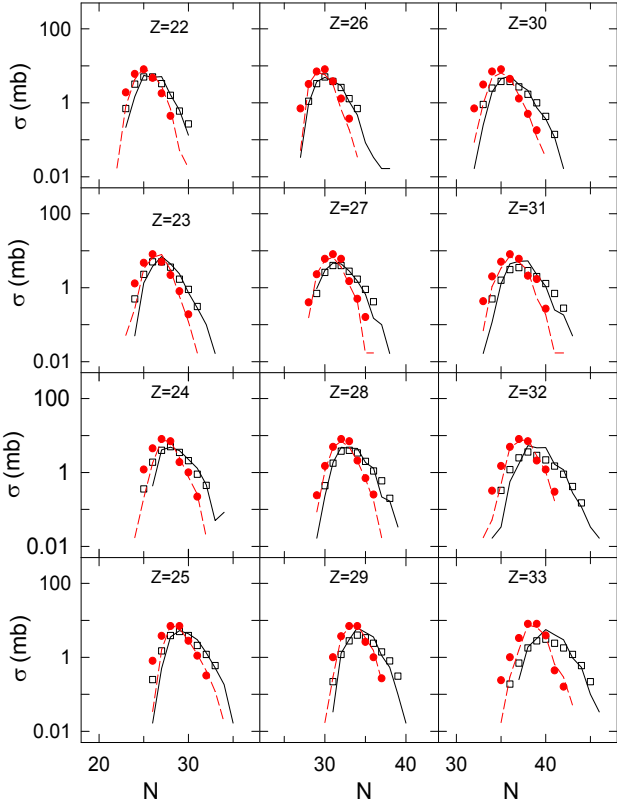


FIG. 5: (color online) As Fig. 4 but for the final fragments with atomic numbers  $22 \leq Z \leq 33$ .

TABLE I: Symmetry-energy coefficient  $\gamma$  chosen for the calculations of the isotopic yield distributions for the listed five element groups on the basis of an optimum reproduction of the experimental results for the two projectile cases.

Z intervals	$^{112}Sn$ $\gamma$ (MeV)	$^{124}Sn$ $\gamma$ (MeV)
Z=10-17	16	16
Z=18-25	19	18
Z=26-31	21	20
Z=32-37	23	19
Z=38-45	25	18

more violent collisions. The global behavior of  $\gamma$  as a function of the fragment mass is, therefore, fully consistent with the impact-parameter dependence deduced from the exclusive ALADIN data for fragmentations at 600 MeV/nucleon. Studied there as a function of the bound charge  $Z_{\text{bound}}$  used for impact-parameter sorting, the symmetry-term coefficient was found to decrease rapidly with increasing multiplicity of fragments and light particles from the decay of the excited spectator systems. Interpreted as resulting from the overall reduced density at breakup and from the hot environment modifying fragment properties, this observation is shown here to extend into the regime of medium-size fragment

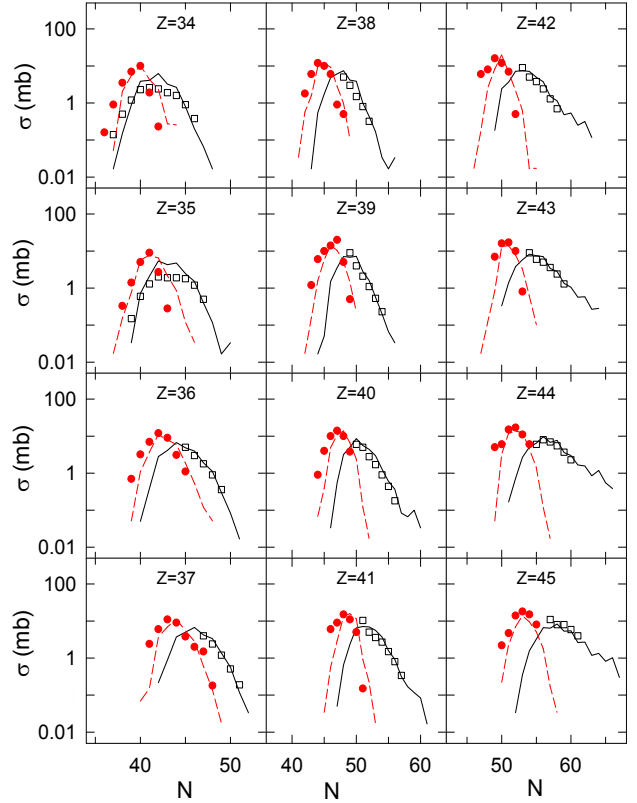


FIG. 6: (color online) As Fig. 4 but for the final fragments with atomic numbers  $34 \leq Z \leq 45$ .

production up to about  $Z = 30$ .

A more quantitative comparison shows that the present  $\gamma = 16$  MeV deduced for  $Z = 10 - 17$  corresponds approximately to the result for the bin of reduced bound charge  $0.6 < Z_{\text{bound}}/Z_0 < 0.8$  of the ALADIN data. Bins of smaller reduced  $Z_{\text{bound}}$  exhibit fragment spectra that decrease as a function of  $Z$  with average values  $< Z > \approx 10$  and below. The symmetry-term coefficient  $\gamma$  determined for these more central bins continues to drop to considerably smaller values [6].

In the same study, it was also explicitly shown that the required coefficient  $\gamma$  is smaller than what could be expected by including a surface-symmetry term into the model. Four different parametrizations were used to calculate an effective symmetry energy, averaged over the experimental set of partitions observed in a particular  $Z_{\text{bound}}$  bin. The smaller fragments produced at higher excitations cause indeed the effective mean symmetry term to decrease with decreasing  $Z_{\text{bound}}$  but at a slower rate than that resulting from the analysis of the experimental data [6].

A similar comparison can be made for the present case. By using the volume symmetry and surface symmetry coefficients  $a_{\text{sym}}^{\text{vol}} = 28.1$  MeV and  $a_{\text{sym}}^{\text{surf}} = 33.2$  MeV of the

Myers and Swiatecki mass formula [31] in the expression

$$\gamma_{\text{eff}} = a_{\text{sym}}^{\text{vol}} - a_{\text{sym}}^{\text{surf}}/A^{(1/3)} \quad (5)$$

effective symmetry-term coefficients may be obtained that explicitly reflect the surface effect. For the bin of smallest fragments studied here,  $Z = 10 - 17$ , typical mass numbers are  $A = 30$  at the end of the de-excitation sequence (cf. panel  $Z = 14$  in Fig. 4) or masses around  $A = 34 - 38$  of the hot sources populating this bin (as given by the SMM calculations). The corresponding  $\gamma_{\text{eff}} = 17.4$  MeV for  $A = 30$  and  $\gamma_{\text{eff}} = 18.0$  MeV for  $A = 36$  are not much but distinctly larger than the  $\gamma = 16$  MeV deduced from the data (Table I) in full agreement with the trends reported in Ref. [6].

The usefulness of such a comparison has to be judged with some caution because the shell correction terms used in the Myers and Swiatecki mass formula are ignored here and, as stated above, the standard symmetry-term coefficient  $\gamma = 25$  MeV is needed to obtain similar results as with a standard evaporation that uses only ground-state masses. Another problem is that, for hot nuclear fragments in the dense environment, the neutron and proton distributions at the surface of the fragments can be different from the case of cold isolated nuclei. The coefficients  $a_{\text{sym}}^{\text{vol}}$  and  $a_{\text{sym}}^{\text{surf}}$  may change in the multifragmentation case. At the present status of the analyses of such experiments it is, therefore, reasonable to consider the evolution of only one symmetry energy coefficient.

Of particular interest are the lower values  $\gamma \approx 19$  MeV obtained for  $Z \geq 32$  and  $^{124}\text{Sn}$  (Table I). In a possible interpretation, this observation may be related to a nuclear structure effect. Shell effects are properly taken into account in the SMM for the ground-state masses which are restored at the end of the secondary de-excitation. At earlier stages of the de-excitation sequence, however, the liquid-drop description is used without shell effects which is adequate at high excitations. The decay chains ending with the heaviest fragments do not start from a very high excitation energy. As shown in Ref. [39], a change of the symmetry-energy coefficient permits a good description of the discontinuities of ground state masses near shell boundaries in a liquid-drop description. A switch to  $\gamma = 14$  MeV is shown to account for the 2-neutron separation energies of nuclei above the neutron shell closure and to correspond to the modification of nuclear properties towards extreme neutron richness. In the present case, the heaviest product nuclei from  $^{124}\text{Sn}$  have neutron numbers  $N \geq 50$  while those from  $^{112}\text{Sn}$  are below  $N = 50$ . A weak persistence of shell effects may thus be indicated for the production of the heaviest fragments. It refers to moderate excitations, lower than in typical multifragmentation events. The enriched neutron environment may have an additional influence which can be expected to grow in importance as one moves closer to the neutron drip-line. In particular, short-range correlations, leading to proton-neutron pairs, may effectively result in decreasing the symmetry energy [40]. New fragmentation and multifragmentation experiments with neutron-

rich secondary beams will be important to resolve these questions.

As discussed previously, multifragmentation reactions can lead to hot nuclei embedded in the dense environment of other nuclear species, with all fragments being in chemical equilibrium [3, 5, 6]. In the present case, the multifragmentation regime covers approximately the production of nuclei with atomic number  $Z < 30$ . A similar composition of nuclear matter is also typical for certain astrophysical sites at subnuclear densities ( $\rho \lesssim 0.1\rho_0$ ) as it is, e.g., temporarily realized during the collapse and explosion of massive stars [20].

For this reason, the extraction of the symmetry energy of hot nuclei from laboratory experiments can contribute to the understanding of astrophysical processes which directly depend on it, mainly the electron capture and neutrino induced reactions. The latter ones, in particular, are crucial for the electron fraction of and the energy deposition in star matter which influence the dynamics of supernova explosions. As shown in Ref. [2], a reduced symmetry coefficient  $\gamma$  affects the density dependent electron capture rates on hot nuclei. The present analysis confirms the trend of a decreasing symmetry energy as one approaches conditions comparable to the multifragmentation regime in agreement with previous findings [3, 5, 6, 12, 13, 15, 17]. The apparent shift and broadening of the isotope mass distributions can be naturally explained by a reduced  $\gamma$  coefficient. Model studies (see, e.g., Refs. [40–42]) suggest that it is more likely the reduced density and the influence of the environment, rather than the increased temperature, which are responsible for such a modification of the properties of hot nuclei. This is confirmed by recent relativistic Thomas-Fermi calculations which show that a weak decrease of the symmetry-energy coefficient of hot nuclei as a function of the temperature is associated with a large increase of the occupied volume [43]. Fully microscopic many-body calculations may be able to clarify this evolution.

#### IV. CONCLUSIONS

It has been shown that the isotopically resolved yield distributions in the range of atomic numbers  $10 \leq Z \leq 45$  from the fragmentation of  $^{124}\text{Sn}$  and  $^{112}\text{Sn}$  projectiles measured with the FRS at 1 GeV/nucleon are well reproduced with statistical calculations in the SMM framework. The good agreement observed with parameters and source distributions obtained previously in the analysis of ALADIN fragmentation data for similar reactions at 600 MeV/nucleon supports the universal properties of the ensemble of excited spectator systems produced during the dynamical stage of the reaction. The previously observed need for a reduction of the symmetry-energy parameter  $\gamma$  for the description of intermediate-mass fragments from the multifragmentation regime has been confirmed and found to extend into the regime of heavier

product species.

The isotopic distributions of the heavier groups of products from the  $^{112}\text{Sn}$  fragmentation are centered close to the evaporation-attractor line while those of heavier products from  $^{124}\text{Sn}$  are located further away. The memory of the neutron-richness of the initial projectile system is seen to be preserved for all isotope distributions. Their location as a function of the neutron number as well as their widths were shown to be mainly sensitive to the symmetry-energy parameter  $\gamma$ . Besides the general trend of a decreasing  $\gamma$  with decreasing fragment mass, i.e. with increasing violence of the collision, it is found that a slightly reduced  $\gamma$  value, with respect to  $^{112}\text{Sn}$ , is required for reproducing the mass distributions of the heaviest fragments from the  $^{124}\text{Sn}$  decay. This observation is tentatively interpreted as being caused by a weak persistence of shell effects in the production of these fragments at moderate excitation energies.

More generally, the obtained results demonstrate the feasibility of investigating in the laboratory the properties of nuclear species at subnuclear densities and surrounded by other species in the freeze-out environment.

Experiments of this kind will be particularly useful and necessary for nuclei far from the stability line. They can be expected to provide us with experimental inputs to the determination of the nuclear equation of state and of the nuclear compositions and matter properties in astrophysical environments of extreme isospin.

### Acknowledgments

Fruitful discussions with A. Kelić-Heil are gratefully acknowledged. This work was supported by TUBITAK (Turkey) with project number 113F058. A.S.B. is supported by the GSI Helmholtzzentrum für Schwerionenforschung GmbH and Hessian initiative for scientific and economic excellence (LOEWE) through the Helmholtz International Center for FAIR (HIC for FAIR). R.O. thanks GSI for hospitality and YÖK (Yüksekokretim Kurulu) for supporting his short visit to GSI in the summer of 2013.

---

[1] J. M. Lattimer and M. Prakash, *Astrophys. J.* **550**, 426 (2001), and references therein.

[2] A. S. Botvina and I. N. Mishustin, *Nucl. Phys. A* **843**, 98 (2010).

[3] A. S. Botvina, O. V. Lozhkin, and W. Trautmann, *Phys. Rev. C* **65**, 044610 (2002).

[4] A. Ono, P. Danielewicz, W. A. Friedman, W. G. Lynch, and M. B. Tsang, *Phys. Rev. C* **68**, 051601(R) (2003).

[5] A. Le Fèvre et al., *Phys. Rev. Lett.* **94**, 162701 (2005).

[6] R. Ogul et al., *Phys. Rev. C* **83**, 024608 (2011).

[7] V. Föhr et al., *Phys. Rev. C* **84**, 054605 (2011).

[8] J. P. Bondorf et al., *Phys. Rep.* **257**, 133 (1995).

[9] A. S. Botvina and I. N. Mishustin, *Phys. Lett. B* **294**, 23 (1992).

[10] A. S. Botvina et al., *Nucl. Phys. A* **584**, 737 (1995).

[11] H. Xi et al., *Z. Phys. A* **359**, 397 (1997).

[12] G. A. Souliotis et al., *Phys. Rev. C* **75**, 011601(R) (2007).

[13] S. Hudan et al., *Phys. Rev. C* **80**, 064611 (2009).

[14] T. X. Liu et al., *Phys. Rev. C* **69**, 014603 (2004).

[15] R. Ogul et al., *J. Phys. G: Nucl. Part. Phys.* **36**, 115106 (2009).

[16] N. Buyukcizmeci et al., *Acta Physica Polonica B* **42**, 697 (2011).

[17] N. Buyukcizmeci et al., *J. Phys. G: Nucl. Part. Phys.* **39**, 115102 (2012).

[18] R. P. Scharenberg et al., *Phys. Rev. C* **64**, 054602 (2001).

[19] S. Das Gupta and A. Z. Mekjian, *Phys. Rev. C* **57**, 1361 (1998).

[20] N. Buyukcizmeci et al., *Nucl. Phys. A* **907**, 13 (2013).

[21] A. S. Botvina, A. S. Iljinov, and I. N. Mishustin, *Sov. J. Nucl. Phys.* **42**, 712 (1985).

[22] A. S. Botvina et al., *Nucl. Phys. A* **475**, 663 (1987).

[23] M. D'Agostino et al., *Phys. Lett. B* **371**, 175 (1996).

[24] N. Bellaize et al., *Nucl. Phys. A* **709**, 367 (2002).

[25] S. P. Avdeyev et al., *Nucl. Phys. A* **709**, 392 (2002).

[26] S. Fritz, et al., *Phys. Lett.* **B461**, 315 (1999).

[27] V. E. Viola, K. Kwiatkowski, J. B. Natowitz, and S. J. Yennello, *Phys. Rev. Lett.* **93**, 132701 (2004).

[28] N. Eren et al., *Eur. Phys. J. A* **49**, 48 (2013).

[29] D. Henzlova et al., *J. Phys. G: Nucl. Part. Phys.* **37**, 085010 (2010).

[30] N. Buyukcizmeci et al., *Eur. Phys. J. A* **25**, 57 (2005).

[31] W. D. Myers and W. J. Swiatecki, *Nucl. Phys.* **81**, 1 (1966).

[32] A. S. Botvina, A. S. Iljinov, and I. N. Mishustin, *Nucl. Phys. A* **507**, 649 (1990).

[33] C. Scheidenberger et al., *Phys. Rev. C* **70**, 014902 (2004).

[34] J. A. Urbon, S. B. Kaufman, D. J. Henderson, and E. P. Steinberg, *Phys. Rev. C* **21**, 1048 (1980).

[35] W.-c. Hsi et al., *Phys. Rev. C* **60**, 034609 (1999).

[36] P. Napolitani et al., *Phys. Rev. C* **70**, 054607 (2004).

[37] K. Sümmerer and B. Blank, *Phys. Rev. C* **61**, 034607 (2000).

[38] R. J. Charity, *Phys. Rev. C* **58**, 1073 (1998).

[39] N. Buyukcizmeci, A. S. Botvina, J. Pochodzalla, and M. Bleicher, *Phys. Rev. C* **88**, 014611 (2013).

[40] A. Carbone, A. Polls, and A. Rios, *Eur. Phys. Lett.* **97**, 22001 (2012).

[41] Bao-An Li and Lie-Wen Chen, *Phys. Rev. C* **74**, 034610 (2006).

[42] S. Typel, G. Ropke, T. Klahn, D. Blaschke, and H.H. Wolter, *Phys. Rev. C* **81**, 015803 (2010).

[43] Z. W. Zhang, S. S. Bao, J. N. Hu, and H. Shen, *Phys. Rev. C* **90**, 054302 (2014).